Flight Test Instrumentation for Loads and Aeroelastic Analyses of a High Altitude, Long Endurance, Solar Electric Aircraft

A. Voß[1], M. Tang[2], J. Sinske[3]
DLR - German Aerospace Center, Institute of Aeroelasticity, 37073 Göttingen, Germany

This work presents the flight test instrumentation for loads and aeroelastic measurements of an extremely light weight and highly flexible aircraft. Because the aircraft is very elastic, the validation of the aeroelastic modeling is essential. Therefore, the aircraft has a comprehensive flight test instrumentation dedicated to the measurement of loads and the elastic response. The measurement equipment, comprising strain gages, accelerometers, temperature sensors and an inertia measuring unit, is presented in detail. Three demonstrations of application are shown with the aircraft on the ground, in preparation for flight testing: online monitoring of strains during ground handling, measurement of rigid body motion during the taxi test and acceleration measurements during the ground vibration test.

I. Introduction

The HAP-alpha (High Altitude Platform) is a very light weight, high altitude and long endurance aircraft (HALE) designed to stay airborne and hold position for several days at an altitude between FL450 and FL800. Carrying optical measurement equipment, this allows scientists to make observations of the earth continuously for a long period of time. This is an advantage compared to satellites, which typically pass the same spot only every couple of days and fly much higher, leading e.g. to a lower optical resolution. The ability to start and land allows to re-configure and re-locate the aircraft for new and different missions. In addition, purchase and operation costs of an

Figure 1: 3D rendering of the HAP-alpha

1 Research Engineer, Institute of Aeroelasticity, arne.voss@dlr.de
2 Research Engineer, Institute of Aeroelasticity, martin.tang@dlr.de
3 Team Lead, Institute of Aeroelasticity, julian.sinske@dlr.de

aircraft are expected to be much lower compared to those of a satellite, including the infrastructure (airfield vs. spaceport).

A 3D rendering image of the HAP-alpha configuration, currently under development at the DLR [13], is shown in Figure 1. The idea is to create an extremely light weight aircraft (m_{design} = 136 kg) that flies very slowly (V_{EAS} = 9.0 to 11.0 m/s) but is highly efficient in terms of propulsion and aerodynamic performance (AR = 20) and is powered by solar electric energy. A team of specialists from different flight-physical disciplines designed this aircraft [8–10,29–31,31] on the edge of the physically possible. Because many design aspects are driven by aeroelasticity [24–26], the validation of the aeroelastic modeling is essential and the aircraft has a comprehensive flight test instrumentation (FTI) dedicated to the measurement of loads and the elastic response of the aircraft. This paper presents the selected FTI equipment and then shows three examples of application with the aircraft on the ground - in preparation for the first flight.

Although a few comparable aircraft are under development by various companies, scientific publications are rare and most of the following sources are press statements, newspaper articles, etc. This is in contrast to DLR's own development HAP-alpha, where much literature is published by the researchers working on the project (see above). A good general overview of high-altitude platform systems and their possible applications is given by Grest [40]. Aircraft that already achieved their first flight include the Atmos by Kea Aerospace [32,41] and the Swift SULE [43], both with a surprisingly similar design. A scaled demonstrator was flown by India's National Aerospace Laboratories (NAL) [42]. BAE selected a slightly different design for their PHASA-35 [12] and also passed their first flight successfully. Structural dynamic aspects of the Airbus Zephyr are presented by Benassi and Aquilini [2], but the paper reveals little details. An accident report on Zephyr's in-flight break-up [1] shows the challenges of operating such an aircraft. Many large companies such as Google [7] and Facebook [3,5,6] were interested as well, but quickly stopped their projects. NASA's prototype Helios and the Solar Impuls are similar at a first glance, but differ in concept and mission. To the authors' best knowledge, there are no publications with respect to flight testing of such a vehicle from any of the companies.

II. Validation Strategy for the Aeroelastic Modeling / Scope of Measurements

The aeroelastic modeling comprises individual models for aerodynamics, mass, stiffness and the flight controller, coupled in the aeroelastic simulation software LoadsKernel [19,20]. The numerical simulation models are described in detail in previous publications [24–26] while this section focuses on expected uncertainties and on the validation strategy of the models. Generally speaking, all models are idealizations of the real aircraft and subject to uncertainties. For example, important details might be missing in the simulation models, calculations, approximations and estimates of quantities could deviate form reality, or parts of the aircraft are simply not manufactured as specified.

The **flight controller** is developed and validated independently [29–31] and then included in the aeroelastic simulations via a functional mock-up unit (FMU). Its commands, e.g. as a reaction to a gust, are accepted as a given.

The **aerodynamic** panels methods, vortex lattice (VLM) and doublet lattice method (DLM) [18,21], are fully applicable due to the slow flight speed leading to a low Mach number (Ma < 0.3) and the slender tube-type fuselage is expected to generate nearly no lift compared to the remaining lifting surfaces. From a loads perspective, the lift distribution in span-wise direction is most important while other quantities such as drag or roll-yaw-coupling are less important. For this aircraft, the author is confident in the aerodynamic modeling as long as the geometry and airfoils are correct. In addition, results were compared against higher fidelity simulations from the aerodynamic design team and showed a good agreement.

During the design phase, larger uncertainties are expected in the **mass** modeling, because only preliminary estimates can be used as the final mass of a component or system is only known once it is build. Once the masses are established, it's more a question of bookkeeping. The residuals between calculated and measured total mass are currently lower than 200g and less than 1.0mm for the center of gravity.

The largest uncertainties are expected in the structural **stiffness** model. The FE model consists mainly of beam elements, which is justified due to the slender, beam-like primary structure. Note that more detailed models are used e.g. for the sizing of the components, while for aeroelastic applications, the focus is on the structural dynamic behavior of the overall aircraft. Possible sources of error on the modeling side are for example the material properties, the calculation of equivalent area moments or the laminate set-up. Obviously, the same errors can occur

on the manufacturing side, leading to an aircraft not build to the specifications (it's a hand-manufactured prototype). In addition, many small, local structural details are omitted or idealized during the modeling. The validation includes two stages: First, a static wing bending test was performed with the a wing prototype. From the deflections under a known loading, bending and torsional stiffness properties were derived and the simulation model was adjusted slightly. Second, a ground vibration test (GVT, see Figure 2) was performed with the whole aircraft to identify the structural dynamic characteristics in terms of eigenfrequencies and mode shapes. This yields information on the modal stiffness and mass distribution, leading again to model updates [22].

The combination of aerodynamics, structure, mass and flight control can only be validated by **flight test**, which is currently in preparation. Special maneuvers are selected, including 1-3-2-1-1 commands of the elevator, aileron sweeps or rudder doublets. The control surface commands are recorded and will be fed as playback signals into the time domain simulation of the free-flying, elastic aircraft. To allow for a meaningful comparison and validation of the aeroelastic models, sufficient measurement data is needed. Therefore, the sensor quantity and distribution over the aircraft is important so that all parts of the aircraft are covered. Different sensors and measurement techniques are helpful to confirm the agreement / disagreement of flight test and simulation from different perspectives. This approach is in line with previous experience from the Discus 2c sailplane [27]. The following quantities will be measured during flight:

- rigid body motion
- elastic response of the aircraft
- loads of the aircraft (section loads, e.g. wing root bending moment)

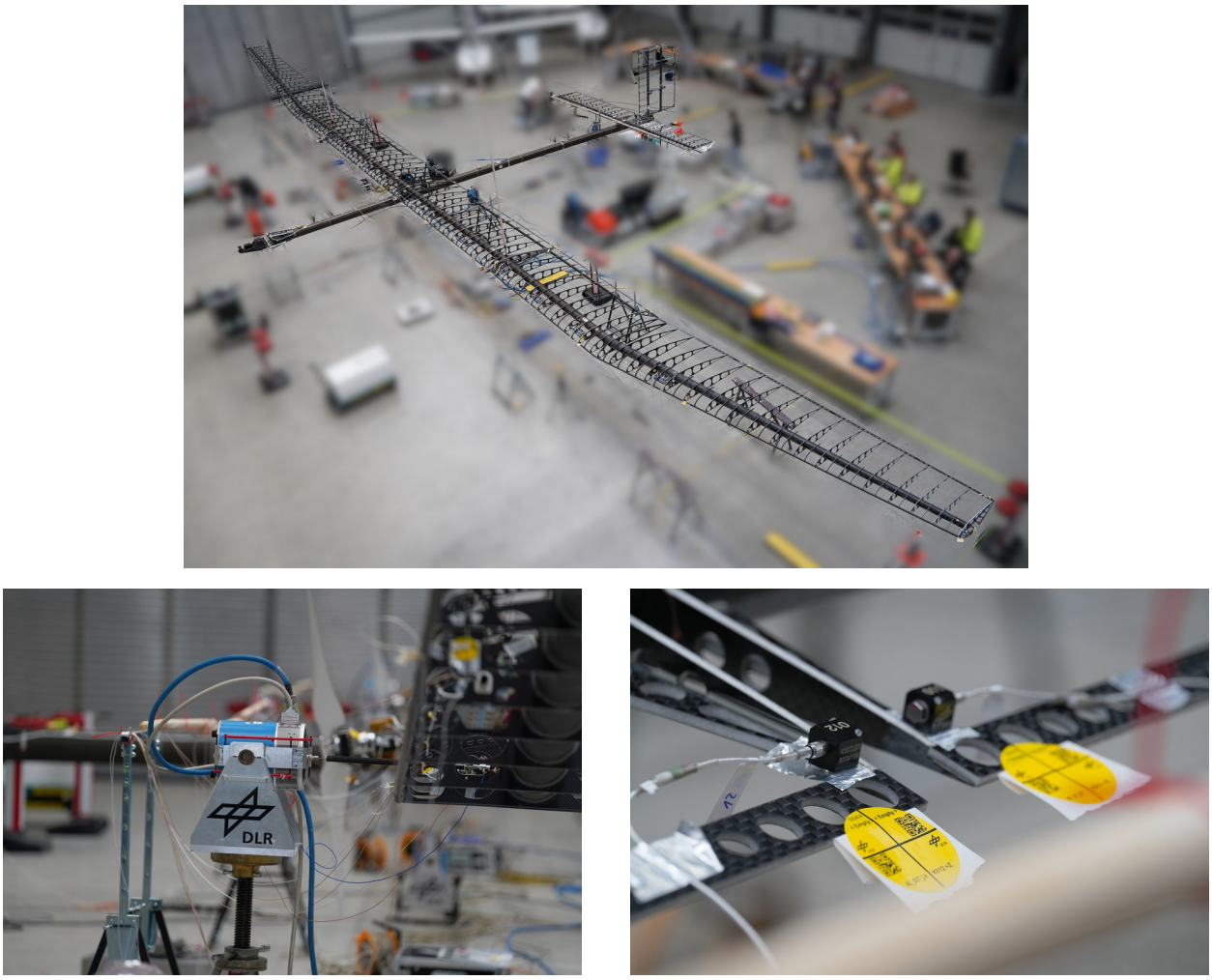

Figure 2: The aircraft during ground vibration test (top), excited by elector-magnetic shakers (left), vibrations of the primary structure measured by accelerometers (right)

For the rigid body motion, quantities such as the GNSS position, altitude, flight speed, accelerations, rates and angles can be compared. They will be recorded by an inertia measuring unit (IMU) and will be completed by data from the aircraft flight computer, which also provides the pilot commands, actuator deflections and air data as an input for the numerical simulations. The elastic response of the aircraft can be measured by accelerometers, distributed e.g. along the wing of the aircraft. Because the maneuvers are expected to be comparativly slow and will include low frequencies, micro-electromechanical systems (MEMS) sensors are favored over piezoelectric accelerometers. For section loads, only an indirect measurement is possible, for example via strain gages. This assumes a linear relationship and requires a calibration procedure, described in Section VII in more detail. In addition, the strain gages will be used for an online monitoring with respect to structural stress/strength during ground handing, see Section IV.

III. Equipment Selection and Sensor Distribution

Strain gages are placed at ten selected locations on the primary structure, see Figure 3. The sensors are typically located on the top, bottom, front and rear side of the tube-type main spar, see Figure 4. They are wired in such a way that at each location, there is

- one bending bridge for bending moments M_x,
- one shear bridge for shear forces F_z and
- one torsional bridge for torsional moments M_y.

This set-up represents the most interesting quantities from a loads perspective (bending and torsion moments M_x and M_y and shear force F_z), measured at three locations along the wings (WR1, WR2, WR3 and WL1, WL2, WL3). At the empennage, strain gages are installed at the root of the horizontal and vertical tail (HR1, HL1 and VT1). Finally, one monitoring station is placed on the rear fuselage (FUS2) to observe the empennage as a whole. For consistency checks, the aircraft is equipped symmetrically.

The strain gages are selected from the M-Series [11] by HBM and include sensors in 0/90° layout (1-TM16-6/350GE) and in +/-45° layout (1-XM46-6/350GE). They were chosen for their large temperature range (-200 to +300 °C) and their thermal expansion coefficient, which is adjusted to quartz glass (0.5 ppm/K). Remember that the thermal expansion of a carbon fiber structure is generally very low, but depends on the laminate set-up and thus changes from component to component. The bridges are wired in such a way that they should not be influenced by temperature changes (Patent 10 2025 129 237 [19]). Still, the strain gages are insulated by 3mm Depron foam and covered by a thin, metal-coated foil (the same as in a first aid kit). This set-up dampens the heat transfer via radiation and convection. In addition, PT100 temperature elements [35] are placed next to the strain gages at the wing and HTP root to monitor any fluctuations of temperature during flight. The following requirements were taken into consideration for the system selection:

- Size and weight, ideal: small and very light-weight
- Versatility: strains, accelerations, temperatures
- Mature and proven design for reliable measurements
- Bandwidth for about 60 channels at 100 or 128 Hz
- External time synchronization with third party equipment
- Ease of use, intuitive user interface and software design
- Power consumption and supply (28V)

With this background, the Wireless Sensor Networks by MicroStrain was chosen, see Figure 5. The system comprises one WSDA-2000 [39] gateway which acts as a base station, collects data from the wireless sensor nodes, has a local storage (upgraded to 32 GB) and provides time synchronization between nodes. The base station can be accessed via USB or Ethernet using the software SensorConnect, the DataDownloader or via a Python interface. For convenience, a small industrial wifi router RUT200 [37] is added to the system to allow for wireless access to the WSDA-2000 to configure the system, to start a measurement, etc. During a measurement, each sample receives a timestamp by the sensor node and all sensor nodes are synchronized by the base station with +/-50 microseconds (according to the manufacturer), which is more than sufficient considering a target sample rate of 128 Hz. Next to the gateway, ten SG-Link-200-OEM [38] strain sensors are used, located in direct proximity to the measurement location. Each sensor node supports three channels, which matches perfectly with the three measurement bridges per

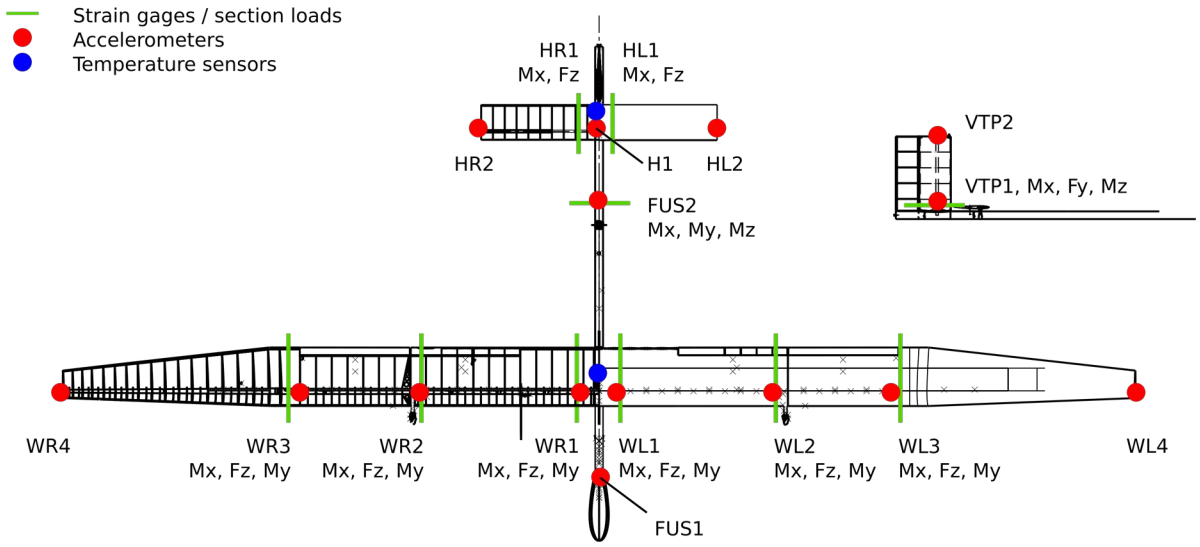

Figure 3: Sensor distribution over the aircraft

location. For the acceleration measurements, fifteen G-Link-200-OEM [34] sensors are installed, which have an on-board triaxial MEMS accelerometer. The sensors are mounted on small frames such that their axis align with the body axis of the aircraft. Note that due to bandwidth limitations, not all axis are recorded for all locations, e.g. along the wing, accelerations in z-direction are more interesting than in y-direction. The name 'OEM' indicates that the sensors come without a housing, leading to a weight of only ca. 16g (sensor + mounting frame). Temperatures are recorded by two RTD-Link-200 [36] sensors, which support up to 6 channels each. The circuit board was extracted from its housing and installed on the aircraft using a small and light 3D printed mounting frame. Finally, one 3DM-GX5-GNSS/INS [33] inertia measuring unit is installed in the payload bay and connected to the WSDA-2000 by cable. Next to the rigid body motion, it provides a GNSS time signal, which is used to set the clock of the WSDA-2000, which in turn synchronizes all sensor node. This is a very elegant way to synchronize with third party measurements, as long as they use GNSS time as well. Even though the measurement system is a commercial off-the-self solution with a proven design and support by the manufacturer, the system was subject to a comprehensive checkout phase with multiple tests:

- Power supply + consumption check
- Communication range test
- Swing set-up (sinusoidal motion) to check internal time synchronization between two nodes
- Frequency response functions of amplitude and phase of accelerometers, mounted on a calibration table
- Strain measurement: reproduce earlier results with imc CRONOSflex system (high-end laboratory measurement system, reference)

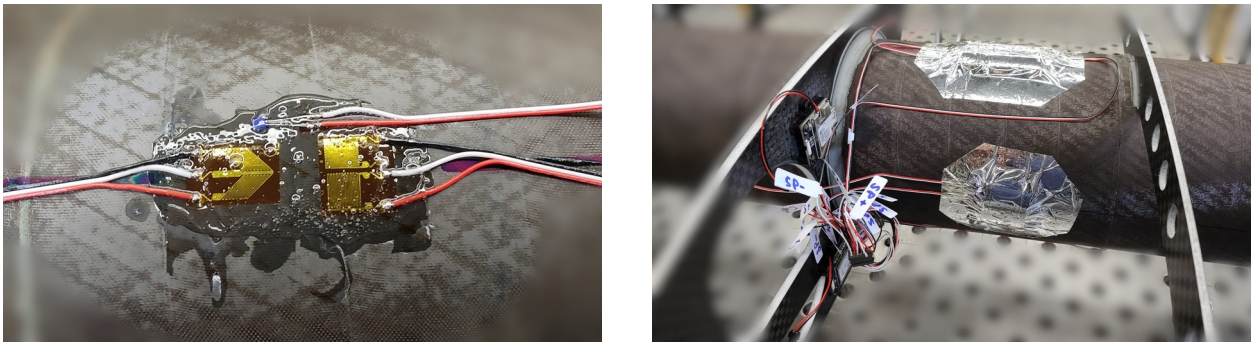

Figure 4: Strain gages on the primary wing structure during installation (left) and with protective cover (right)

Figure 5: Components of the Wireless Sensor Network by MicroStrain: WSDA-2000, G-Link-200, SG-Link-200, 3DM-GX5-GNSS/INS, RTD-Link-200 [44]

- Comparison of two strain sensors with strain gages under exact same loading
- Test of strain sensors with sweep and random signals from Simcenter SCADAS Mobile (high-end laboratory measurement system, reference)
- Amplitude check of measured voltages
- Temperature signal plausibility check
- System qualification in climate chamber (-70°C to +80°C for bending bridge, -40°C to +80°C for measurement hardware)
- Electromagnetic emission and exposure tests
- External time synchronization with third-party systems
- Plausibility check of IMU data (mounted on bicycle + “flight path” reconstruction)

The total mass of the measurement system is split in two categories, 686g of equipment is installed in the payload bay and 787g are distributed over the aircraft, including the strain gages and their installation material. The power supply is not considered as the power bus is already in place. The wireless communication is probably the biggest feature and drawback at the same time: Like in all wireless applications, data packages can be dropped. However, the wireless protocol is lossless in the sense that 50% of the packages may be dropped. In case the connection is lost completely, the sensor nodes have a local storage and will continue sampling, and once connection is re-established, the data transmission resumes and eventually catches up with real time. Unfortunately, the frequency band (2.405 to 2.480 GHz) coincides with the frequencies typical used for wifi and bluetooth and most environments are full of laptops, headsets, computer mouses, smartphones, etc. While the transmission protocol itself is lossless, it was found to be difficult to set up a measurement with all 27 sensor nodes, because there are always a few nodes which are not responding in that very moment.

Figure 6: WSDA-2000 gateway, IMU, GNSS antenna and wifi router combined to one unit (left), installed in the payload bay at the aircraft nose (right)

Figure 7: HAP-Alpha on launch vehicle during taxi test

IV. Online Monitoring of Strains During Ground Handling

On the ground, an overloading and damage of the extremely light-weight structure might occur due to unintentional mishandling. From the raw data obtained from the strain gages (in microvolts), local strains ϵ in the material are calculated using the following relationship

$$\epsilon = \frac{4 \cdot U_{\text{sens}}}{k \cdot N \cdot U_{\text{supply}}}, \tag{1}$$

with $k = 2.30$ for all strain gages involved in this set-up, the bridge number $N = 4.0$ for shear and torsion and $N = 2 \cdot (1 + \nu)$ for bending as well as the supply voltage $U_{\text{supply}} = 2.5V$ and the measured voltage U_{sens}. For meaningful strains, the tara / zero value is important. After the installation of the strain gages, the components were carefully placed on a flat surface such that the loading should be as close to zero as possible, and the tara values were recorded. In this way and using equation (1), voltages can be calculated that correspond to the maximum allowable strains of the material. As the measurement data can be accessed online via wifi, this enables an online monitoring of the strains while the aircraft is tested or simply move around in the hangar. Figure 8 shows a screenshot taken during ground handling tests, limit loads are indicated by orange color while red indicates a loading beyond ultimate load. The two plots show the readings from the bending sensors along the left and right wing. In this test, the aircraft is picked up by two cranes and lifted onto the start vehicle for the first time. One can see a few distinct steps in the measurement data as the aircraft is lifted, but the strains are well within the limit loads – as intended.

Figure 8: Screenshot of online strain monitoring using the SensorConnect software

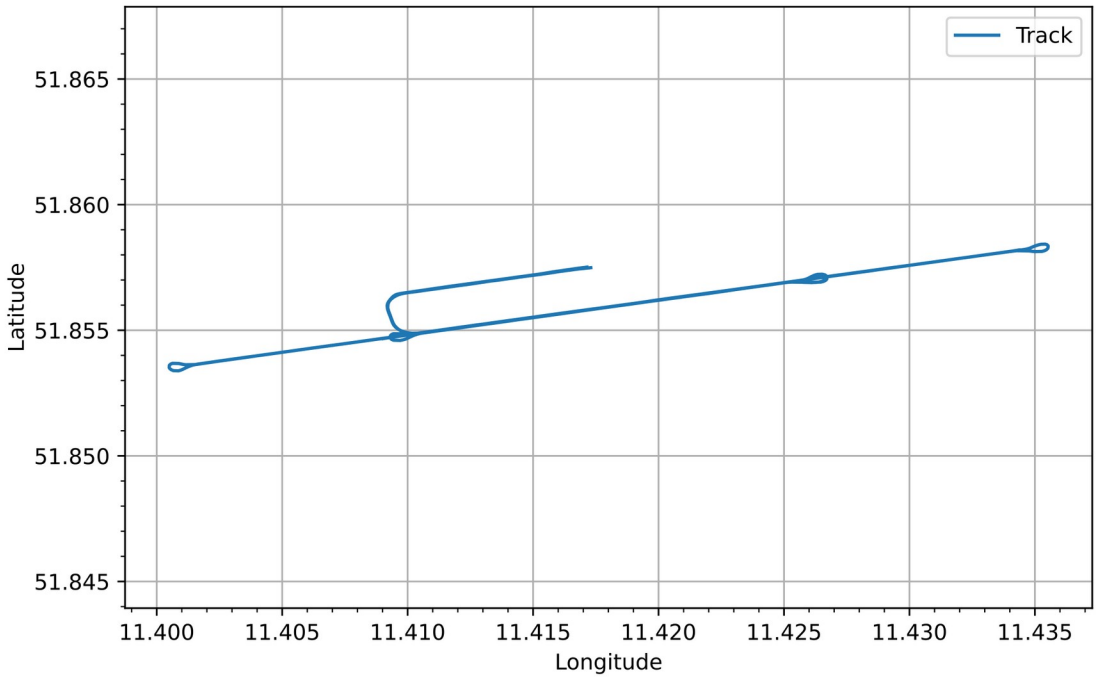

Figure 9: Recording of track on ground during taxi test

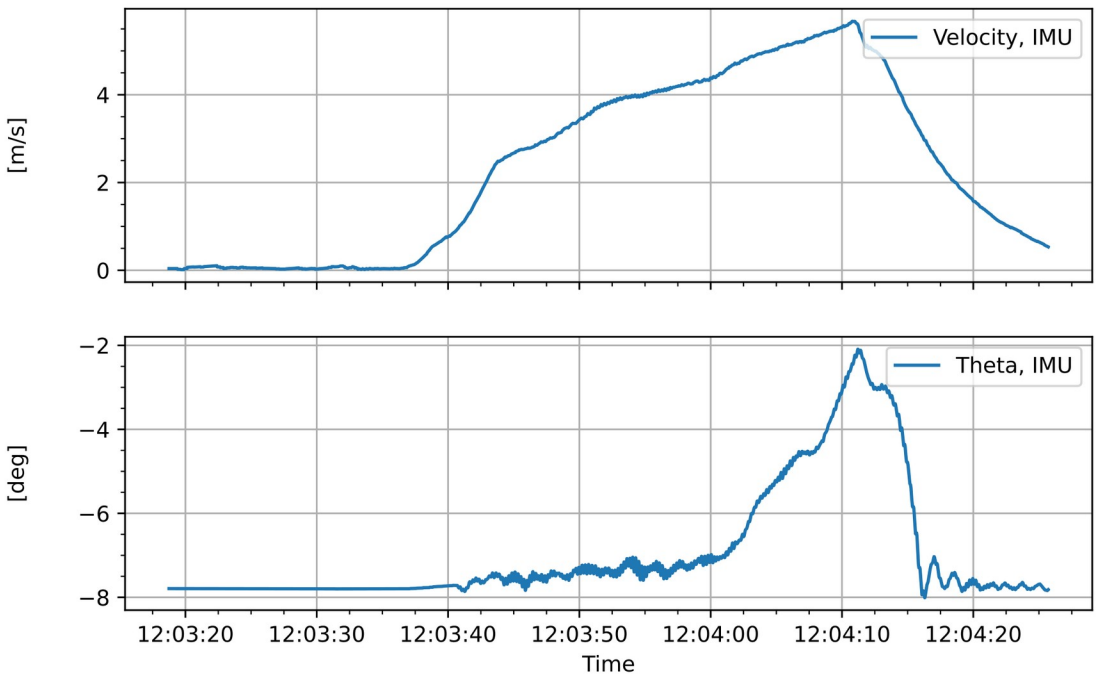

Figure 10: Velocity and pitch angle during pitch-up event

V. Rigid Body Motion During Taxi Tests

The aircraft is launched from a vehicle as shown in Figure 7. To familiarize with this approach, a taxi test is performed. The aircraft was monitored closely from a chase vehicle as well as by observation of the online data from the flight test instrumentation. After leaving the hangar, multiple trips up and down the runway were performed at different speeds. While the taxi test was uneventful from a loads and aeroelastic perspective, it provides a good opportunity for plausibility checks of the rigid body motion. The recorded track over ground is shown in Figure 9. Good agreement was observed between track, yaw angle and yaw rate, for example when turning around at the end of the runway. Figure 10 shows an unexpected pitch-up incidence while the pitch-lock was disengaged by mistake. The incidence starts with the aircraft at stand-still and in nominal position with a negative (nose down) pitch angle. At 12:03:37h the launch vehicle accelerates and the aircraft suddenly starts to pitch up, which can be explained by the center of gravity above the pivot axis and the increasing drag of the vertical tail at higher speeds. The vehicle driver, informed via radio, slowed down again and any damage could be averted. The incidence shows that the rigid body motion is captured in sufficient detail by the IMU and will provide good data for the comparison of simulation and flight test.

VI. Acceleration Measurements During Ground Vibration Test

A GVT has been conducted in order to characterize the aircraft by means of modal parameters [22]. The enables the validation of the structural model of the aircraft. Additional accelerometers are mounted on the structure and for the excitation electro-magnetic shakers have been employed. In addition, the internal accelerometers depicted in Figure 3 are measured and validated. For this purpose, only the measured accelerations of the FTI sensors are analyzed with unknown input forces with the Stochastic Subspace Identification (SSI) algorithm [16]. Application of this methodology have been shown for wind tunnel tests and flight tests [4,15,17].

A random excitation run with one shaker in z-direction under the fuselage is chosen for the following comparison, because most symmetrical modes of the aircraft are well excited. An excellent agreement of the fundamental eigenfrequencies was found as can be seen by the comparison in Table 1. Next to the frequencies, also the mode shapes are the same, as shown in Figure 11 for the first inplane and out-of-plane wing bending. Note that one FTI sensor is missing on the left outer wing. Higher order modes are more difficult to identify due to the smaller number of sensors (FTI: 15 sensors, GVT: > 80 sensors), leading to a lower spatial resolution. Because the FTI sensors are only placed along the wing span and not in chord direction, torsional modes can’t be captured with this set-up. The excellent agreement of the eigenfrequencies and mode shapes identified with the GVT hardware means that the FTI can be used for additional, small-scale vibration tests, e.g. with manual hand excitation. This is useful to identify any changes in the structural dynamic behavior of the aircraft, for example after the skin is installed, when the aircraft is modified at a later stage, and possibly even during flight by excitation from natural turbulence.

Mode	GVT [Hz]	FTI [Hz]
2n wing bending	0.99	0.99
2n wing inplane	1.57	1.57
HTP roll	3.53	3.52
4n wing bending	3.63	3.63

Table 1: Comparison of frequencies measured with GVT and FTI sensors

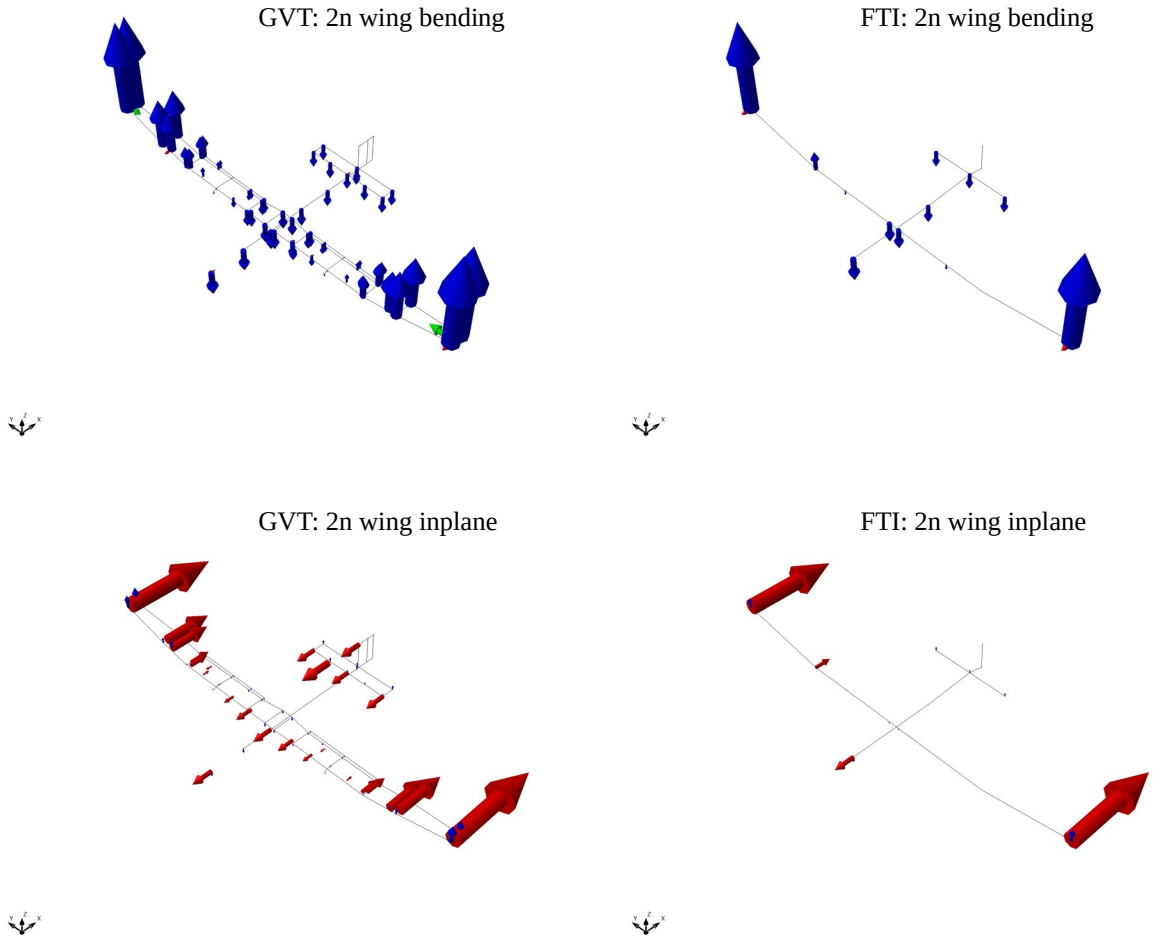

Figure 11: Comparison of first inplane and out-of-plane wing bending shapes

VII. Outlook: Load Measurements Based on Strains

To measure loads based on strains, the assumption is a linear relationship between strains $\boldsymbol{\mu}$ and section loads $\mathbf{v}$, such that

$$\mathbf{v} = \boldsymbol{\beta} \cdot \boldsymbol{\mu}. \tag{2}$$

The task is to find a calibration matrix $\boldsymbol{\beta}$ (also called Skopinski-matrix) by application of a known loading. During the flight test, the strains $\boldsymbol{\mu}$ are recorded, followed by a reconstruction of the section loads $\mathbf{v}$ that must have acted on the structure. The theoretical background is described by Skopinski et al. [14] already in 1954, the application is the tricky part. Pre-tests have been performed on a 3m wing segment with very good results [28]. A calibration is only meaningful after installation of the foil-type skin, which, although it is very thin, contributes to the primary, load-carrying structure. To enable easy access to all systems, wires, etc. during the ground tests, this step will be performed just before flight test.

VIII. Conclusions and Steps Towards Flight Testing

This work presents a flight test instrumentation for the extremly light weight, high altitude and long endurance aircraft HAP-alpha. The aircraft is designed on the edge of what is physically possible and many design aspects are

driven by aeroelasticity, meaning that the validation of the aeroelastic modeling is essential. Therefor, the aircraft has a comprehensive but very light flight test instrumentation dedicated to the measurement of loads and the elastic response. The measurement equipment, comprising strain gages, accelerometers, temperature sensors and an inertia measuring unit, was presented in detail. Three demonstrations of application are shown, not in a laboratory set-up but on the real aircraft and under typical conditions with the only exception that the aircraft was (still) on ground. The results are plausible, so that the authors are confident in the measurement set-up and are waiting for the first flight.

The first flights in lower altitude will take place in DLR's National Experimental Test Center for Unmanned Aircraft Systems located in Cochstedt, Germany, while flights in higher altitude are planned for Kiruna, Sweden or Tawhaki, New Zealand. Once the flight test of the aircraft itself is completed, two different measurement systems (an optical camera system and a synthetic aperture radar) will be installed as payload and tested in the lower stratosphere, followed by first scientific missions.

Acknowledgments

The equipment selection and the checkout of the measurement system was performed with the support and the existing experience by the two experimental departments of the DLR Institute of Aeroelasticity. The sensor installation was performed in close coordination with the DLR Institute of Lightweight Systems while the integration of the measurement hardware was supported by the DLR Institute of Flight Systems. The first author is very grateful for the support from all parties involved.

References

[1] Australian Transport Safety Bureau, "In-flight break-up involving Airbus Zephyr unmanned aerial vehicle", Australian Transport Safety Bureau, Canberra, Australia, ATSB Transport Safety Report AO-2019-056, Sep. 2020.

[2] Benassi, L., and Aquilini, C., "The Structural Dynamics of Flying Non Stop for 100 Days", in *18th International Forum on Aeroelasticity and Structural Dynamics*, Savannah, Georgia, 2019.

[3] Bolandhemmat, H., "Flight Control System Design for a High Altitude, Long Endurance Airplane: Sensor Distribution and Flexible Modes Control". Facebook Research.

[4] Böswald, M., Govers, Y., Jelicic, G., and Buchbach, R., "Online monitoring of flutter stability during wind tunnel testing of an elastic wing with pylon and engine nacelle within the HMAE1 project", in *International Forum on Aeroelasticity and Structural Dynamics 2019, IFASD 2019*, Savannah, GA (USA), 2019, https://elib.dlr.de/128030/.

[5] Colas, D., Roberts, N. H., and Suryakumar, V. S., "HALE Multidisciplinary Design Optimization Part I: Solar-Powered Single and Multiple-Boom Aircraft", presented at the AIAA Aviation, Atlanta, Georgia, 2018, https://doi.org/10.2514/6.2018-3028.

[6] Colas, D., Roberts, N. H., and Suryakumar, V. S., "HALE Multidisciplinary Design Optimization Part II: Solar-Powered Flying-Wing Aircraft", presented at the AIAA Aviation, Atlanta, Georgia, 2018, https://doi.org/10.2514/6.2018-3028.

[7] Gibbs, S., "Google's Titan drones to take flight within months", *The Guardian*, 03-Mar-2015, https://www.theguardian.com/technology/2015/mar/03/googles-titan-drones-to-take-flight-within-months.

[8] Hasan, Y., Fezans, N., and Voß, A., "Landing Simulation of a High-Altitude Platform with Skid-Type Landing Gear - Flight Procedure, Controller and Loads", presented at the ICAS Congress, Stockholm, Sweden, 2022, https://elib.dlr.de/191048/.

[9] Hasan, Y. J., Fezans, N., and Voß, A., "Flight Mechanical Analysis of a Very Flexible High-Altitude Platform Under Uncertainty Considerations", presented at the 34th Congress of the International Council of the Aeronautical Sciences, Florence, Italy, 2024.

[10] Hasan, Y. J., Roeser, M. S., Hepperle, M., Niemann, S., Voß, A., Handojo, V., and Weiser, C., "Flight mechanical analysis of a solar-powered high-altitude platform", *CEAS Aeronaut J*, Nov. 2022, https://doi.org/10.1007/s13272-022-00621-2.

[11] HBM, "Katalog für Dehnungsmessstreifen", https://www.hbm.com/fileadmin/mediapool/hbmdoc/technical/S01264.pdf.

[12] Kay, A., "PHASA-35 First Flight | Ground-breaking solar powered unmanned aircraft makes first flight", *BAE Systems | International*, 17-Feb-2020. [Online]. Available at: https://www.baesystems.com/en/article/ground-breaking-solar-powered-unmanned-aircraft-makes-first-flight. [Accessed: 20-Feb-2020].

[13] Nikodem, F., "Overview of the DLR High Altitude Platform and Scientific Potential of the Technology Demontrator HAP-alpha", presented at the Deutscher Luft- und Raumfahrtkongress 2023, Stuttgart, Deutschland, 2023,

https://elib.dlr.de/198509/.
[14] Skopinski, T. H., Aiken, W. S., and Huston, W. B., “Calibration of strain-gage installations in aircraft structures for the measurement of flight loads”, National Advisory Committee for Aeronautics. Langley Aeronautical Lab, Langley Field, VA, Technical Report NACA-TR-1178, Jan. 1954, http://ntrs.nasa.gov/search.jsp?R=19930090978.
[15] Soal, K. I., Schwochow, J., Volkmar, R., Tang, M., Thiem, C., Govers, Y., Böswald, M., Kier, T., Süelözgen, Ö., Guerin, N., Teubl, D., Bartasevicius, J., Vanek, B., Toth, S., and Nagy, M., “Flutter flight testing: Using operational modal analysis to identify, track and predict flutter for safe and efficient flight test campaigns”, presented at the International Forum on Aeroelasticity and Structural Dynamics, IFASD 2024, Den Haag, Niederlande, 2024, https://conf.ifasd2024.nl/proceedings/display_manuscript/119.htm.
[16] Van Overschee, P., and De Moor, B., *Subspace Identification for Linear Systems*. Boston, MA: Springer US, 1996, https://doi.org/10.1007/978-1-4613-0465-4.
[17] Volkmar, R., Soal, K., Govers, Y., and Böswald, M., “Experimental and operational modal analysis: Automated system identification for safety-critical applications”, *Mechanical Systems and Signal Processing*, vol. 183, p. 109658, Jan. 2023, https://doi.org/10.1016/j.ymssp.2022.109658.
[18] Voß, A., “An Implementation of the Vortex Lattice and the Doublet Lattice Method”, Institut für Aeroelastik, Deutsches Zentrum für Luft- und Raumfahrt, Göttingen, Germany, Technical Report DLR-IB-AE-GO-2020-137, Oktober 2020, https://elib.dlr.de/136536/.
[19] Voß, A., “Loads Kernel User Guide”, Institut für Aeroelastik, Deutsches Zentrum für Luft- und Raumfahrt, Göttingen, Germany, Technical Report DLR-IB-AE-GO-2020-136, Jul. 2020, https://elib.dlr.de/140268/.
[20] Voß, A., “LoadsKernel Release 2025.01”, 08-Jan-2025. [Online]. Available at: https://zenodo.org/records/14617118. [Accessed: 03-Feb-2025].
[21] Voß, A., “PanelAero Release 2024.02”, 13-Feb-2024. [Online]. Available at: https://zenodo.org/doi/10.5281/zenodo.8343766. [Accessed: 05-May-2025].
[22] Voß, A., Buchbach, R., Soal, K., Volkmar, R., Thiem, C., Sinske, J., and Niemann, S., “HAP-alpha: Model Updating and the Influence on Loads and Aeroelasticity”, presented at the International Forum on Aeroelasticity and Structural Dynamics, Göttingen, Germany, 2026.
[23] Voß, A., and Handojo, V., “Tragflächen-Primärstruktur mit Dehnungsmessstreifen”, Deutsches Patent- und Markenamt, patent number 10 2024 129 237, 15-Sep-2025.
[24] Voß, A., Handojo, V., Weiser, C., and Niemann, S., “Preparation of Loads and Aeroelastic Analyses of a High Altitude, Long Endurance, Solar Electric Aircraft”, presented at the AEC2020 Aerospace Europe Conference, Bordeaux, France, 2020, https://elib.dlr.de/133496/.
[25] Voß, A., Handojo, V., Weiser, C., and Niemann, S., “Results from Loads and Aeroelastic Analyses of a High Altitude, Long Endurance, Solar Electric Aircraft”, *Journal of Aeroelasticity and Structural Dynamics*, vol. 9, no. 1, pp. 1–22, Jan. 2022, https://doi.org/10.3293/asdj.2021.58.
[26] Voß, A., Koch, C., Niemann, S., Mantei, Marius, Handojo, V., and Weiser, C., “Transition From Preliminary to Detailed Design of a Highly Elastic Solar Electric Aircraft”, presented at the International Forum on Aeroelasticity and Structural Dynamics, Madrid, Spain, 2022, https://elib.dlr.de/186492/.
[27] Voß, A., and Ohme, P., “Dynamic maneuver loads calculations for a sailplane and comparison with flight test”, *CEAS Aeronautical Journal*, vol. 9, no. 3, pp. 445–460, Apr. 2018, https://doi.org/10.1007/s13272-018-0300-9.
[28] Voß, A., Soal, K., Sinske, J., Meier, D., Niemann, S., Nickle, J., and Hanke, M., “Pre-Test of a Light-Weight CFRP Wing Segment of a High Altitude Platform for In-flight Load Measurements Based on Strains”, presented at the Deutscher Luft- und Raumfahrtkongress, Bremen, 2021, https://doi.org/10.25967/550028.
[29] Weiser, C., and Ossmann, D., “Baseline Flight Control System for High Altitude Long Endurance Aircraft”, in *AIAA SciTech 2022 Forum*, San Diego, USA, 2022, https://arc.aiaa.org/doi/10.2514/6.2022-1390.
[30] Weiser, C., Ossmann, D., and Pfifer, H., “Robust Path-Following Control for High-Altitude Long-Endurance Aircraft”, *Journal of Guidance, Control, and Dynamics*, vol. 7, no. 46, pp. 1416–1424, May 2023, https://arc.aiaa.org/doi/full/10.2514/1.G007326.
[31] Weiser, C., Schulz, S., Voß, A., and Ossmann, D., “Attitude Control for High Altitude Long Endurance Aircraft Considering Structural Load Limits”, presented at the AIAA SCITECH 2023 Forum, National Harbor, Maryland, 2023, https://doi.org/10.2514/6.2023-0106.
[32] “6,000ft Flight Completes Low Altitude Test Campaign”, *Kea Aerospace*, 02-Dec-2024. https://www.keaaerospace.com/news-and-events/6000ft-flight-completes-low-altitude-test-campaign/.
[33] “Datasheet 3DM-GX5-GNSS/INS”, *MicroStrain by HBK*. [Online]. Available at: https://www.microstrain.com/inertial-sensors/3dm-gx5-45. [Accessed: 06-Sep-2024].
[34] “Datasheet G-LINK-200-OEM”, *MicroStrain by HBK*. [Online]. Available at: https://www.microstrain.com/wireless-

sensors/g-link-200-oem. [Accessed: 22-Jul-2024].
[35] “Datasheet M222”, *Yageo Nexensos*. [Online]. Available at: https://www.heraeus.com/de/hne/sensor_products/wired_sensors/medium_temperature_range/page_product_detail.html. [Accessed: 22-Jul-2024].
[36] “Datasheet RTD-Link-200”, *MicroStrain by HBK*. [Online]. Available at: https://www.microstrain.com/wireless-sensors/rtd-link-200. [Accessed: 22-Jul-2024].
[37] “Datasheet RUT200”, *Teltonika*. [Online]. Available at: https://teltonika-networks.comde/de/products/routers/rut200. [Accessed: 06-Sep-2024].
[38] “Datasheet SG-Link-200-OEM”, *MicroStrain by HBK*. [Online]. Available at: https://www.microstrain.com/wireless-sensors/sg-link-200-oem. [Accessed: 22-Jul-2024].
[39] “Datasheet WSDA-2000”, *MicroStrain by HBK*. [Online]. Available at: https://www.microstrain.com/wireless-sensors/wsda-2000. [Accessed: 06-Sep-2024].
[40] “High-Altitude Platform Systems - Joint Air Power Competence Centre”, 21-Jul-2022. https://www.japcc.org/articles/high-altitude-platform-systems/.
[41] “Media Release: Kea Aerospace Achieves Historic Stratospheric Flight”, *Kea Aerospace*, 11-Feb-2025. https://www.keaaerospace.com/news-and-events/media-release-kea-aerospace-achieves-historic-stratospheric-flight/.
[42] “Meet HAPS: India’s very own UAV that can fly 20 km high and float for months”, *The Indian Express*, 10-Feb-2024. https://indianexpress.com/article/india/meet-haps-indias-very-own-uav-that-can-fly-20-km-high-and-float-for-months-9153929/.
[43] “Swift announces its SULE uncrewed aircraft flies above 55,000 feet”, *Military Aerospace*, 18-Nov-2024. [Online]. Available at: https://www.militaryaerospace.com/uncrewed/article/55243431/swift-announces-sule-uas-tops-55000-feet. [Accessed: 28-Nov-2024].
[44] “Wireless DAQ Systems”, *HBK World*. [Online]. Available at: https://www.hbkworld.com/en/products/instruments/wireless-daq-systems. [Accessed: 01-Oct-2025].